JOURNAL OF GEOPHYSICAL RESEARCH, VOL. 113, B04306, doi:10.1029/2007JB005112, 2008

Identification of seismic precursors before large earthquakes: Decelerating and accelerating seismic patterns

Panayotis Papadimitriou[1]

Received 13 April 2007; revised 16 December 2007; accepted 15 January 2008; published 22 April 2008.

[1] A useful way of understanding both seismotectonic processes and earthquake prediction research is to conceive seismic patterns as a function of space and time. The present work investigates seismic precursors before the occurrence of an earthquake. It does so by means of a methodology designed to study spatiotemporal characteristics of seismicity in a selected area. This methodology is based on two phenomena: the decelerating moment release (DMR) and the accelerating moment release (AMR), as they occur within a period ranging from several months to a few years before the oncoming event. The combination of these two seismic sequences leads to the proposed decelerating-accelerating moment release (DAMR) earthquake sequence, which appears as the last stage of loading in the earthquake cycle. This seismic activity appears as a foreshock sequence and can be supported by the stress accumulation model (SAM). The DAMR earthquake sequence constitutes a double seismic precursor identified in space and time before the occurrence of an earthquake and can be used to improve seismic hazard assessment research. In this study, the developed methodology is applied to the data of the 1989 Loma Prieta (California), the 1995 Kobe (Japan), and the 2003 Lefkada (Greece) earthquakes. The last part of this study focuses on the application of the methodology to the Ionian Sea (western Greece) and forecasts two earthquakes in that area.

Citation: Papadimitriou, P. (2008), Identification of seismic precursors before large earthquakes: Decelerating and accelerating seismic patterns, *J. Geophys. Res.*, *113*, B04306, doi:10.1029/2007JB005112.

1. Introduction

[2] On the assumption that earthquakes do not occur randomly in space and time, the study of seismic patterns is fundamental to understanding the phenomenon of earthquake preparation. Thus far investigations of empirical and theoretical descriptions of spatiotemporal patterns of seismicity have focused mainly on three observations: seismic quiescence, the accelerating seismic energy/moment release (AMR), and the stress interactions between earthquakes. *Wyss and Habermann* [1988], for example, have reported precursory quiescence, lasting for months or years before the occurrence of large earthquakes. *Bufe and Varnes* [1993] have observed accelerating seismic moment release within a broader area around the epicenter of a future earthquake. *Reasenberg and Simpson* [1992], *King et al.* [1994], *Stein* [1999], and *Toda and Stein* [2003] have observed local triggering effects due to stress changes caused by previous earthquakes.

[3] Seismic rate changes prior to the occurrence of an earthquake have also been reported. *Mogi* [1969], for example, has proposed the "doughnut pattern," according to which increased seismicity during a certain period before the occurrence of a strong event concentrates around the periphery of the oncoming rupture zone, while the rupture zone itself is relatively quiescent. *Wiemer and Wyss* [1997] have noted that asperities may be characterized by low *b* values and high stress regimes. They identified places susceptible to future large earthquakes by estimating the local recurrence time from *a* and *b* values. On the other hand, *Sobolev and Tyupkin* [1999] have advanced the region-time-length (RTL) method, which investigates seismicity pattern changes prior to large earthquakes. Their research indicates that seismic quiescence anomalies generally start a few years before the occurrence of large events.

[4] Studies focusing on precursory seismicity rate changes before large earthquakes have revealed an increase in seismic activity over a broad region known as "accelerating moment release" (AMR). The generation of accelerating seismic activity observed before main shocks is considered a critical phenomenon, culminating in a large event [*Sornette and Sornette*, 1990; *Sykes and Jaume*, 1990; *Sornette and Sammis*, 1995; *Bowman and King*, 2001]. Various studies on seismicity and fracturing indicate that earthquake distributions exhibit fractal (scale-invariant) properties on various scales [*Kagan and Knopoff*, 1980; *Huang and Turcotte*, 1988; *Kagan and Jackson*, 1991]. In such cases earthquakes are considered self-similar fractal processes, implying scale-invariance, and are described by the power law time-to-failure equation [*Bufe and Varnes*,

[1]Department of Geophysics, University of Athens, Panepistimiopolis, Zografou, Greece.

0148-0227/08/2007JB005112$09.00

1993]. Studies of regions that indicate an increase of seismicity before the occurrence of large events have been conducted by many researchers [*Saleur et al.*, 1996; *Jaume and Sykes*, 1999; *Rundle et al.*, 2000; *Ben-Zion and Lyakhovsky*, 2002; *Papazachos et al.*, 2002, 2006; *Sammis et al.*, 2004]. *Main* [1999] has examined the range of applicability of the power law equation while *Zoller et al.* [2001] has tested the critical point concept for earthquakes in terms of growing spatial correlation length. Stress changes prior to the Coalinga earthquake have been reported by *Tiampo et al.* [2006], applying the Pattern Informatics technique.

[5] In this study seismological catalogs will be analyzed for possible precursory seismic pattern detection before the occurrence of large earthquakes. The methodology employed in the analysis is based on four different approaches designed to discriminate and quantify spatio-temporal changes, and thus estimate space and time prior to an earthquake. In this work the Benioff strain (the square root of seismic energy release) has been selected to describe changes in space and time through earthquake catalogs. For physical reasons, energy release rather than the Benioff strain is frequently used. The methodology will be applied to the Loma Prieta, Kobe and Lefkada earthquakes. Finally, this study entertains the possibility of two oncoming earthquakes in the Ionian Sea (western Greece).

2. Methodology

[6] On the basis of the study of the spatiotemporal characteristics of seismicity in a selected area, the methodology of this work can reveal both the occurrence time and the epicentral area of a future earthquake. The occurrence time of the oncoming event is estimated using two different methods, the first based on accelerating seismicity, and the second on the temporal distribution of energy release. The identification of the candidate area is estimated also using two different methods, the identification of the critical area, and the spatial distribution of energy release. In the event all four methods indicate seismic precursors, the area is thought to be in a critical state, which indicates that a large event may occur. The four methods are presented below.

2.1. Accelerating Seismicity

[7] Large earthquakes are frequently preceded by variations of regional seismicity. Many efforts have been made to describe precursory phenomena using different analytic functions. *Bufe and Varnes* [1993] noted that a simple power law, the time-to-failure equation derived from damage mechanics, can be used to model the observed seismicity. According to Bufe and Varnes, the seismicity before the 1989 Loma Prieta earthquake can be expressed by the form

$$\frac{ds(t)}{dt} = B \cdot (t_c - t)^{m-1} \tag{1}$$

and by integration

$$s(t) = A - \frac{B}{m}(t_c - t)^m \tag{2}$$

where $s(t)$ is a measure of seismic energy release, called the Benioff strain, t_c is the origin time of the main shock, B is a positive constant and m is a parameter usually less than 1, which represents the degree of accelerating energy release. A is the value of $s(t)$ when $t = t_c$ and represents the final Benioff strain, including the main shock. The observed cumulative Benioff strain at time t is defined as:

$$\varepsilon(t) = \sum_{i=1}^{N(t)} \sqrt{E_i(t)} \tag{3}$$

where E_i is the energy of the ith event and $N(t)$ is the number of events up to time t. To calculate the energy release of an event, the following formula, which is proposed by *Kanamori and Anderson* [1975], is used:

$$\log E = 1.5 * M + 4.8 \tag{4}$$

The parameters of equation (2) are defined by fitting the failure function $s(t)$ to the observed cumulative Benioff strain $\varepsilon(t)$ on the basis of events occurring in the selected area. Using equation (2) it is possible to estimate the degree of acceleration m of the selected area, the magnitude M (from parameter A) and the occurrence time t_c.

2.2. Temporal Variation of Energy Release

[8] The temporal variation of energy release, represented by the quality factor Q_t, is calculated using the moving window technique. The quality factor Q_t is defined as

$$Q_t(t) = \frac{1}{k}\sum_{i=1}^{k} \varepsilon_i(t) \tag{5}$$

where $\varepsilon_i(t)$ is the observed Benioff strain of the ith event and k is a fixed number of selected events. The consecutive values of Q_t are calculated by shifting the moving window through the earthquake catalog. A minimum number of events is required for a reliable calculation (generally $k >$ 60 events), and depends on the density and the M_c of the catalog. The quality factor Q_t is constructed to calculate the mean energy release through the earthquake catalog. In general, this factor must fluctuate around a reference level in the absence of a large earthquake (background level). When an earthquake is approaching, a large anomaly is observed some years before the main event [*Papadimitriou*, 2002, 2004]. The mean temporal variation of Q_t first drops to a minimum level characterized by decelerating seismicity and corresponding to time period ΔT_d (starting from the background and ending with the minimum level). Following, Q_t presents an increase until the occurrence of the main event. During this period Q_t is characterized by accelerating seismicity and corresponds to time period ΔT_a (starting from the minimum level and ending with the occurrence time). The end of this acceleration must asymptotically point to the occurrence time t_c and Q_t (approximately the background level). The total duration of this time period is defined as $\Delta T = \Delta T_d + \Delta T_a$. In addition the acceleration time period ΔT_a is divided into two subperiods: $\Delta T_a = \Delta t_a + \Delta t_i$. The identification time Δt_i represents the last time period before the occurrence time t_c, generally less than 1 year. For a future event Δt_i can only be estimated even though the beginning of Δt_i can be identified by an abrupt change rate. The acceleration period Δt_a extends from the minimum level to the beginning of Δt_i. In this formulation the identification time

Δt_i represents also the time error of the estimated occurrence time t_c. Thus, equation (5) represents the temporal variation of the energy release of a selected area. In the case of an event, Q_t must show two important deviations that correspond to the decelerating and accelerating time periods. The end of the accelerating time period ΔT_a points to the estimated occurrence time t_c with an error of $\pm \Delta t_i$.

2.3. Identification of Critical Area and Time

[9] The identification of the critical area/time for a future earthquake is one of the main objectives in earthquake prediction research. In equation (2), parameter m, which represents the accelerating degree of energy release, can be utilized as an identifier. In order to calculate parameters m, t_c and B (A is fixed), the difference between the observed and theoretical energy release must be minimized via the least squares method:

$$\Delta = \sum_{i=1}^{N(t)} [\varepsilon_i(t) - s_i(t)]^2 = \min \tag{6}$$

At the same time the curvature parameter c is calculated, as proposed by *Bowman et al.* [1998]. This parameter represents the quantification of the degree of acceleration, and is equal to the ratio between the root mean square error of power law fit and the root mean square error of linear fit. By minimizing equation (6) it is possible to evaluate parameters m, c and to estimate the occurrence time of the main event, t_c. For the identification of the critical area/time the quality factor Q_c is defined as

$$Q_c(\vec{x}, t) = amc \tag{7}$$

where the constant α is an amplification factor whose value in the present study is $\alpha = 1.0$, but which could take different values in other applications. The identification of a critical area/time can be based on the grid technique, where the quality factor Q_c is calculated at each node. The quality factor must be less than 1, but becomes critical only for values $Q_c \ll 1$, which permits us to estimate the size of the critical area. By the end of this procedure, the size of the critical area (in case one is found) can be identified and be treated as a pattern recognition process. Thus equation (7) provides the possibility to identify areas in a critical state and to estimate the occurrence time t_c at each node.

2.4. Spatial Distribution of Energy Release

[10] The gridding technique is used to study the spatial distribution of energy release for a selected area divided into a grid of about $\Delta x = 0.02°$ spacing. At each node the quality factor Q_s is calculated for a number of events, situated within a cylindrical volume with radius r, depth distribution between $[h_1, h_2]$, and defined as the sum of all events that occurred at time t_i with epicenter $\vec{x_i}$:

$$Q_s(\vec{x}, t_1, t_2) = \sum_{i=1}^{N(t)} \varepsilon_i(\vec{x_i}, t_i) \tag{8}$$

where $[t_1, t_2]$ is the selected time interval and the selected events have epicentral distances $|\vec{x} - \vec{x_i}| \leq r$. Furthermore, $\varepsilon_i(\vec{x_i}, t_i)$ is the Benioff strain of the ith event and $N(t)$ is the number of the events within the cylindrical volume. Thus, the quality factor Q_s represents the energy release of a certain geographic position. Using equation (8), it is possible to calculate the spatial distribution of energy release. Analyzing the obtained pattern, it becomes possible to discriminate areas of low from those of high energy release. The expectation is that, should an event occur, such an event will most likely occur in the area with low energy release. The area that exhibits low energy release must be correlated to the one presenting seismic quiescence, as well as to the critical area identified in section 2.3, which is calculated independently.

3. Data

[11] Reliable catalogs of seismicity as a function of space, time, and magnitude are necessary to investigate the evolving characteristics of seismic patterns before the occurrence of large events. It is generally assumed that the quality of earthquake catalogs is improving through time, as seismological digital networks are developed worldwide. In fact, seismological catalogs contain increasingly more information concerning small events. As a result, uncertainties of hypocenter parameters are reduced. Nevertheless, problems due to magnitude determination errors and to the existence of aftershocks and swarms still remain. The latter are considered dependent events that can be separated from independent ones by means of different algorithms [*Reasenberg*, 1985; *Smirnov*, 1998]. The goal of these algorithms is to remove all dependent events from each cluster within a given radius and time window, and to replace them by one event with a magnitude equivalent to the total energy released. The resulting declustered catalog must contain a homogeneous data set for detecting seismicity rate changes that reflect tectonic processes instead of changes due to the detection capability. The completeness of the catalog can be estimated on the basis of the power law frequency-magnitude relationship. Thus, the catalog becomes homogeneous above a minimum magnitude M_c. As a result, the cumulative number of earthquakes versus time must be almost linear.

[12] In the present study the above mentioned procedure is applied to three different regions to detect possible seismic precursors. The first application concerns the 1989 Loma Prieta earthquake (California), the second application concerns the 1995 Kobe earthquake (Japan), and the third application concerns the 2003 Lefkada earthquake (Greece). For the identification of accelerating seismicity in a region, earthquakes with magnitude greater than $M_{\min} > 4.5$ are generally used [*Bowman et al.*, 1998; *Papazachos et al.*, 2005]. Thus, in many cases a radius of $R \gg 100$ km is considered in order to obtain enough seismicity. On the basis of fractal properties, in which a large-scale phenomenon can be observed in a smaller-scale, seismicity with magnitude $M_{\min} \geq M_c$ was chosen in this study. For the three selected regions, the catalogs used were provided by NCEDC (Northern California Earthquake Data Center), ISC (International Seismological Centre), and

GINOA (Geodynamic Institute of National Observatory of Athens).

4. Data Processing

[13] Modeling accelerating seismicity by using the original seismological catalog can lead to apparent acceleration, which is generally due to local perturbations (aftershocks, swarms) producing step function changes in the rate of seismicity. To avoid this problem, the catalog must be declustered before any operational process. The consequence of such declustering is that the cumulative Benioff strain becomes linear for the entire region, and the c value is almost 1. After eliminating aftershocks and swarms from the catalogs by applying the *Reasenberg* [1985] algorithm, the completeness of the catalogs was evaluated based on the frequency-magnitude distribution cumulated from above and below. The calculated magnitude completeness for the Loma Prieta, Kobe and Lefkada events is $M_c = 2.4$, $M_c = 2.6$, and $M_c = 3.5$, respectively. More details are presented in Appendix A.

[14] The temporal distribution of energy release is estimated using equation (5). For each critical area the quality factor Q_t is calculated for a time period starting about 10 years before the time of the main event. At the beginning of this time the mean variation of Q_t indicates the mean long-term variation of the energy release (background level) of the selected area. A precursory signal is identified when consecutives values of Q_t indicate a significant deviation from the mean variation until the occurrence of the main event. Parameter k, which is included in equation (5), must be defined in such a way that the discrimination between these time periods is evident. More details are presented in Appendix B.

[15] The detection of seismic precursors can be realized by the identification of precursory events in a space/time window and the definition of the area of interest using simple geometrical shapes, such as circles or ellipses. The gridding technique is used to identify the critical area/time using constant radius R_n. Each node is considered an epicenter, and all events with magnitude equal to or larger than $M_{\min}$ located within its circular/or elliptical area are selected. On the basis of these selected events, the quality factor Q_c is calculated for each node using equation (7). When a set of nodes shows $Q_c \ll 1$, the area is considered critical and its size can be evaluated. If the data is insufficient or if $Q_c > 1$, then Q_c is treated as 1.

[16] A predictive modeling method that uses equations (2) and (3) must estimate four parameters. During the process of estimating them it is possible to find some degree of acceleration, called "apparent acceleration." To quantify this bias, *Mignan et al.* [2006] created random synthetic catalogs using an optimal search algorithm to determine the likelihood that a seismicity sequence could have arisen stochastically. The result of this procedure, expressed by cumulative probability, suggests that any given synthetic catalog has 50% chance of generating an optimal c value of 0.6 or higher, less than 25% when $c \leq 0.5$ and less than 7% when $c \leq 0.4$. The authors conclude that any seismicity sequence with $c \geq 0.6$ is unclear. The statistical significance of these measurements indicates that for c values less than 0.6 the accelerating seismicity is driven by nonrandom processes.

[17] In this study there is no search for an optimal region (the radius of the selected area is constant). Thus the mentioned measurements are taken into account by calculating Q_c and considering only values where $Q_c \ll 1$. Most researchers, when estimating a critical area using an optimal region approach, hold the degree of acceleration constant ($m \approx 0.3$). As such their measurements are based only on c values. When c is almost 1, the Benioff strain rate indicates deceleration or linearity; when $c < 1$, the indication is acceleration. In this study the critical area is estimated by calculating the quality factor Q_c, taking into account both m and c. Parameter m has been included as a significant factor, designating the degree of acceleration. However, only values $0.12 < m < 0.45$ and $c < 0.8$ are considered. For the most part these values are smaller and depend on the specific earthquake. But outside these limits of m, even when $c < 0.6$, the critical area increases and additional small areas appear. The significance of this approach is that the calculation of m yields a more accurate estimation of the occurrence time t_c.

5. Case Studies

[18] The proposed methodology was applied to three earthquakes (Loma Prieta, Kobe, and Lefkada) in three different seismotectonic regions. These earthquakes were selected because they occurred in three of the most active regions and because they have already been studied by different researchers employing different methodologies. This study combines elements of seismic quiescence and accelerating seismicity methodologies, and supplements them with those of decelerating seismicity and spatial energy release. To maintain the independence of the methodology, all three events are studied using different standard seismological catalogs available to the seismological community.

5.1. Accelerating Energy Release

[19] Concerning the factor of accelerating seismicity, the critical point hypothesis is that large earthquakes occur only when the system is in a critical state. Thus seismicity in an area preparing for a large earthquake is expected to increase as a function of power law. Therefore, an area approaching criticality can be identified by optimizing equation (2). This is achieved by fitting this equation with the observed Benioff strain (equation (3)). The $\varepsilon(t)$ must initially be approximately linear, corresponding to the null hypothesis, according to which the seismicity rate is constant at the beginning of the time period. After a certain time seismicity accelerates prior to the main shock. When this happens, the critical exponent m (equation (2)) and the curvature parameter c must be less than 1, to distinguish the curvature of the power law from the straight line over the considered timescale. If seismicity is increasing linearly, parameter c is approximately 1.

[20] Several researchers agree that the magnitude of the main event scales with the logarithm of the radius of the critical region. They have observed similar scaling to the one proposed by *Keilis-Borok and Kossobokov* [1990]. The maximum distance R between the epicenter and its precur-

sors can be expressed by the relation $\log R = 0.44M$ (several times the activated fault length). A possible explanation for this formula is that the energy of the main event scales with the volume of the crust approaching criticality. In the framework of the present study, the maximum distance is obtained by the formula $\log R = 0.4M - 0.6$, which is similar to the one proposed by *Papazachos and Papazachos* [2000]. Nevertheless, this study selects a constant area centered at the epicenter with radius R_n in order to evaluate the critical area. Radius R_n must be less than or equal to the maximum distance R, and its size depends on the seismotectonic characteristics of the region. After the selection of the area, the parameters of equation (2) are calculated by fitting the observed strain (equation (3)) with the theoretical one. In cases where the main event has already occurred, parameters A and t_c are known, and only parameters B, m and c are calculated by minimizing equation (6). In this study only the most recent years, where the temporal distribution of energy release shows large anomalies, are presented.

[21] Figure 1a represents the Benioff strain variation versus time for the 1989 Loma Prieta earthquake. Events were selected for an elliptic area of R_1 = 80 km and R_2 = 120 km centered at the epicenter, magnitude $M_{\min} \geq 3.4$, focal depth $d_i \leq 80$ km and time period Δt = [1986, 1989.26]. The best fit was obtained for the following values: degree of acceleration $m = 0.25$, curvature parameter $c = 0.74$ and occurrence time t_c = 1989.86 (A is fixed). When A and t_c are fixed (t_c = 1989.80) then similar values are found ($m = 0.24$ and $c = 0.75$). The same event was studied by *Bowman et al.* [1998] using a different approach. Comparing the same time intervals, the Benioff strain variation was similar to the one presented in this study. The important point is the presence of three moderate events at the beginning of 1988. The presence of these events, which are included in both studies, produces an abrupt increase in the observed Benioff strain $\varepsilon(t)$, marking a clear acceleration period. This observation will be compared with the one obtained in section 5.2, where the temporal analysis is performed. It should be noted that *Bowman et al.* [1998] used the original catalog, not the declustered one. In order to compare the curves of the observed Benioff strain, this study did the same. In some cases, this procedure is useful because abrupt increases in the observed Benioff strain rate coincide with those observed when conducting a temporal analysis. However, this procedure tends to yield c values greater than those obtained using the declustered catalog.

[22] The Benioff strain variation versus time for the 1995 Kobe event is presented in Figure 1b. Events were selected for a circular area centered at the epicenter of the earthquake with radius R_n = 150 km, magnitude $M_{\min} \geq 3.2$, depth $d_i <$ 80 km and time period ΔT = [1993, 1994.7]. The best fit was obtained for a degree of acceleration $m = 0.21$, curvature parameter $c = 0.61$ and occurrence time t_c = 1995.22 (A is fixed). In case A and t_c are fixed (t_c = 1995.046) $m = 0.18$ and $c = 0.65$. The Benioff strain rate remains approximately constant up to January 1994 when an increase of the strain rate is observed marking the beginning of a clear acceleration period. A second abrupt increase is observed in October 1994 until the occurrence of the main shock.

[23] The variation of the Benioff strain versus time for the 2003 Lefkada earthquake is presented in Figure 1c.

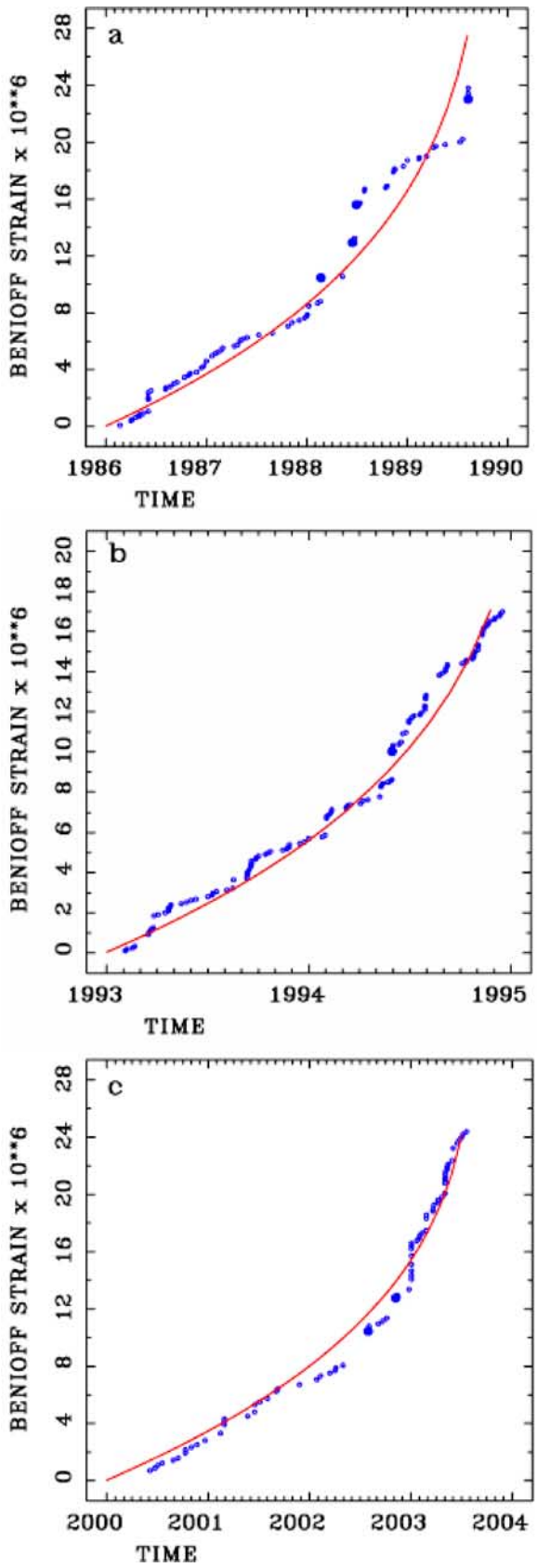

Figure 1. Theoretical (curve) and observed (circles) cumulative Benioff strain variation for the (a) Loma Prieta, (b) Kobe, and (c) Lefkada earthquakes.

Events were selected for an elliptical area of R_1 = 80 km and R_2 = 100 km, magnitude $M_{min} \geq 3.8$, focal depth $d_i <$ 80 km and time period Δt = [2000, 2003.55]. The best fit was obtained for a degree of acceleration m = 0.29, curvature parameter c = 0.45 and occurrence time t_c = 2003.62 (A is fixed). In case A and t_c are fixed (t_c = 2003.62), m = 0.29 and c = 0.45 (the values of m and c are the same because almost identical times were considered). The Benioff strain rate remains approximately constant up to January 2003, when an abrupt increase of the strain rate is observed marking the beginning of a clear acceleration period. It should be noticed that the inclusion of microseismicity ($M \geq M_{min}$) gives more details about the observed strain rate changes some years before the main event. Using such a seismic pattern, the predicted modeling provides a good fit between the observed and synthetic Benioff strain rate, which provides a reliable reading of the predicted parameters.

5.2. Temporal Analysis of Energy Release

[24] The temporal variation of energy release is calculated using the moving window technique in order to analyze the energy release over time ($T \leq 10$ years) before a large event. For a given epicenter, a circular (or elliptical) area of radius $R_n \sim 100$ km is defined, and following, the mean energy release is calculated through the earthquake catalog for a fixed number of k events. The calculation of the temporal variation Q_t is first applied to the Loma Prieta earthquake, setting k = 100. Events were selected for the time period Δt = [1980, 1989.8] and magnitude $M_{min} \geq$ 3.2. The mean value of the temporal variation of Q_t is equal to 6.5 $J^{1/2}$ (background level) for the time interval 1984–1986.5 (Figure 2a). Starting with March 1986, Q_t continuously decreases until January 1988, defining a first time period ΔT_d = [1986.5, 1988.1] characterized by decelerating seismicity. This time period is followed by an increase of energy release until May 1989, defining a second time period Δt_a = [1988.1, 1989.4]. At the end of this period, Q_t exhibits an abrupt increase until the main event, defining a third time period Δt_i = [1989.4, 1989.8]. The last two time periods are characterized by accelerating seismicity. All these time periods are indicated by a horizontal blue line with vertical bars (Figure 2a). The detected seismic precursor has a total duration of about $\Delta T \approx 3.5$ years and is divided into three time periods: the first of decelerating seismicity lasts $\Delta T_d \approx 1.7$ years, the second of accelerating seismicity $\Delta t_a \approx 1.3$ years, and the third of identification time $\Delta t_i \approx 0.5$ years. The identification time Δt_i is separated from the Δt_a because the former is considered critical time (last stage of the earthquake preparation process). The identification time combined with the t_c, which is calculated using equation (2), contributes to higher accuracy in the estimation of the occurrence time. In this case, the end of Δt_i must asymptotically point to t_c. It should be noted that the beginning of Δt_i coincides with the abrupt Benioff strain rate changes mentioned in section 5.1. Thus the estimated occurrence time is t_c = 1989.8 with an error ± 0.5 years.

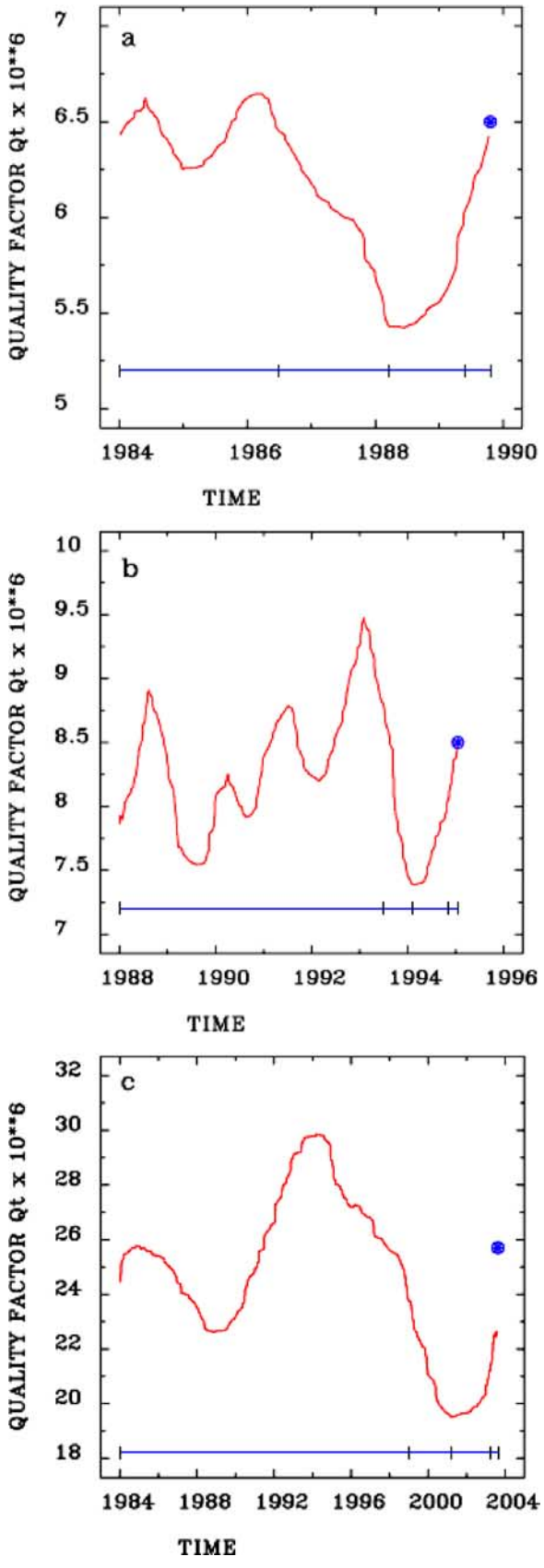

Figure 2. Temporal variation of the quality factor Q_t for the (a) Loma Prieta, (b) Kobe, and (c) Lefkada earthquakes. The star represents the origin time of the main event. The horizontal line marked by vertical bars indicates the time period of background seismicity, ΔT_d, ΔT_a, and ΔT_i.

[25] Following, the calculation of the temporal variation Q_t is applied to the Kobe earthquake, setting $k = 120$. Events were selected for the time period Δt = [1986, 1995.04] and magnitude $M_{\min} \geq 3.2$. Figure 2b represents the temporal variation of Q_t which is equal to 8.5 $J^{1/2}$ for the time period 1988–1993.5. Starting with 1993 the energy level progressively diminishes until January 1994, defining the first decelerating time period ΔT_d = [1993.5, 1994.1]. Following this period, Q_t shows an increase until September 1994, defining a second time period Δt_a = [1994.1, 1994.8]. The third time period extends from the end of the second time period until the occurrence of the event, defining the critical time period Δt_i = [1994.8, 1995.04]. The detected seismic precursors have a total duration of $\Delta T \approx 1.7$ years of which $\Delta T_d \approx 0.7$ years is attributed to decelerating and $\Delta T_a \approx 0.7$ years to accelerating seismicity. The duration of the critical time Δt_i is about 0.3 year, which is also the estimated occurrence time error for this event. In Figure 2b all these time periods are indicated by a horizontal blue line with vertical bars. *Huang et al.* [2001] investigated the characteristics of the seismicity changes associated with the Kobe event using the RTL method. In that study, seismic quiescence was detected at the beginning of 1993; then it reached a minimum in May 1994, and was followed by an activation stage. The temporal variation of Q_t, presented in Figure 2b, clearly indicates the same observation. It should be noted that the beginning of the time period Δt_i coincides with the abrupt Benioff strain rate changes mentioned in section 5.1.

[26] The third application concerns the Lefkada earthquake. The temporal variation of Q_t versus time, setting k = 120, is presented in Figure 2c. Events were selected for the time period Δt = [1980, 2003.6] and magnitude $M_{\min} \geq 3.8$. The mean value of Q_t is equal to 25.7 $J^{1/2}$ for the time interval 1984–1999. It is evident that the energy level after 1995 continuously decreases, something also noticed by *Papazachos et al.* [2004]. In their study, which plotted the number of events as a function of time, seismic quiescence was observed. Starting with January 1999 (background level) Q_t continuously decreases, until it reaches a minimum level in February 2001, defining the first time period ΔT_d = [1999.0, 2001.1]. Following this period an increase of energy level is observed, defining a second time period Δt_a = [2001.1, 2003.2]. Then Q_t presents an abrupt increase, defining a third time period Δt_i = [2003.2, 2003.6]. All these time periods are indicated by a horizontal blue line with vertical bars (Figure 2c). The detected seismic precursors have a total duration of $\Delta T \approx 4.6$ years of which $\Delta t_d \approx 2.1$ years are attributed to decelerating and $\Delta t_a \approx 2.1$ years to accelerating seismicity. The last $\Delta t_i \approx 0.4$ year of accelerating seismicity are defined as critical time, which is also the estimated occurrence time error. It should be noted that the beginning of the time period Δt_i coincides with the abrupt Benioff strain rate changes observed in section 5.1.

[27] Taking into account the above mentioned observations several years before the earthquake, Q_t varies around the background level. Then, Q_t drops to a minimum value, and, some time before the main shock, exhibits an increase. In this pattern the role of parameter k is to discriminate between the background level and the minimum value, thus identifying possible temporal seismic precursors. As a result, the decelerating-accelerating time period turns into a double seismic precursor, and becomes critical some time (usually less than 1 year) before the occurrence of the main shock. For this reason, the accelerating period is divided into two subperiods Δt_a and Δt_i. Finally, the decelerating time period ΔT_d has been observed in virtually all events, and can be related to seismic quiescence observed worldwide.

5.3. Identification of Critical Area and Occurrence Time

[28] In this study, a gridding technique is used to identify precursory seismic patterns in space. The selected region is divided into a grid of 0.25° × 0.25° spacing. Considering circles whose centers are the nodes, and whose radius in the order of $R_n \sim 100$ km, the region is scanned to identify possible areas in which the quality factor Q_c becomes critical ($Q_c \ll 1$). By using this procedure it is possible to find some degree of apparent acceleration. However, as mentioned in section 4, to avoid such a problem the quality factor Q_c must be less than 1 and weighted by parameters m and c. In any other case, $Q_c = 1$ means that no critical area/time is found. The first application concerns the Loma Prieta earthquake where Q_c is calculated using the following criteria: rectangular area 36.0° < latitude < 38.5° and 237.0° < longitude < 240.0°, time period Δt = [1986, 1989.4] and magnitude $M_{\min} \geq 3.4$. With radii R_n ranging from 80 to 140 km a critical area is always identified, the size depending on the selected radius. Figure 3a shows the identified critical area using R_n = 90 km, this value yielding minimum error. In Figure 3a a circle with radius 50 km centered at the epicenter is plotted for any size comparison. The spatial distribution of $Q_c \leq 0.3$ reveals a reduced area (red-violet color) whose size is comparable to the circle surface. During this procedure the occurrence time t_c is also estimated, and the result is presented in Figure 4a. The light blue color represents times less than 1989.4 or greater than 1990.5, which correspond to values of $Q_c = 1$. The green-blue colors represent times close to the origin time and correspond to values of $Q_c \leq 0.25$. For these times, the mean value of the degree of acceleration is $m = 0.14$, the curvature parameter $c < 0.65$ (around the epicenter), and the estimated error of occurrence time t_c is less than 1 month if May 1989 is chosen as the last time period in the earthquake catalog.

[29] The second application concerns the Kobe earthquake where Q_c is calculated using the following criteria: rectangular area 33° < latitude < 36° and 133° < longitude < 137°, time period Δt = [1993, 1994.8], magnitude $M_{\min} \geq 3.1$. Figure 3b shows the identified critical area using R_n = 150 km. The spatial distribution of $Q_c \leq 0.3$ reveals a reduced area (red-violet color) whose size is less than that of a circle surface of radius R = 50 km. In Figure 4b the estimated occurrence time t_c is presented. The light blue color represents times less than 1994.8 or greater than 1995.9, which correspond to values of $Q_c = 1$. The green-blue colors represent times close to the origin time and correspond to values of $Q_c \leq 0.25$. For these times, the mean value of the degree of acceleration is $m = 0.21$, the curvature parameter $c < 0.56$ and the estimated error of occurrence time t_c is less than 1 month if September 1994 is chosen as the last time period in the earthquake catalog.

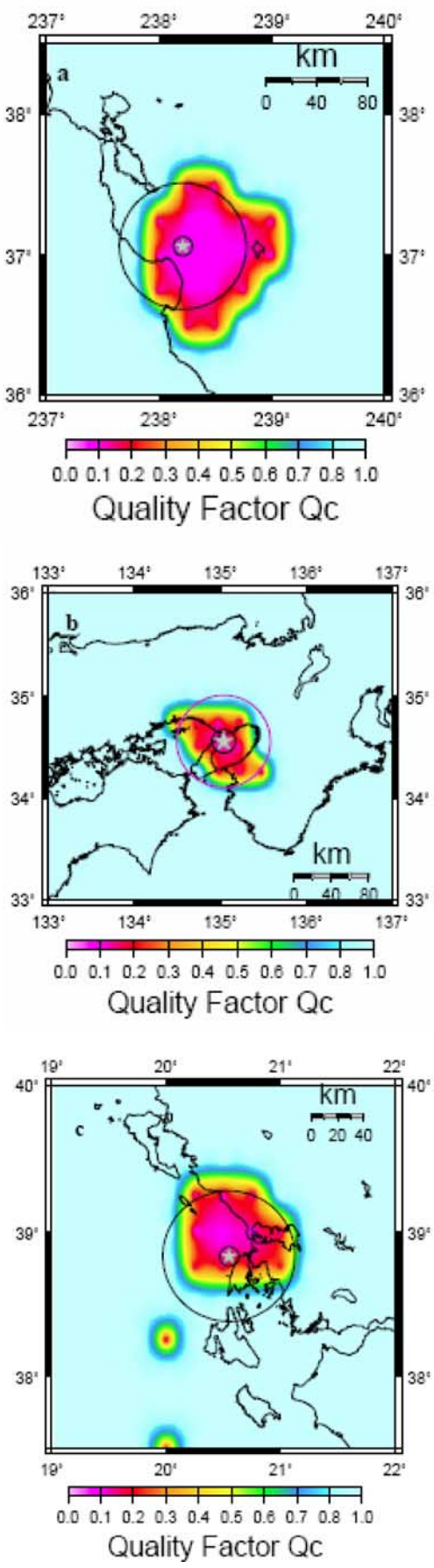

Figure 3. Spatial distribution of the quality factor Q_c. Identification of critical area for the (a) Loma Prieta, (b) Kobe, and (c) Lefkada earthquakes. The star indicates the epicenter of the main event.

[30] The third application concerns the Lefkada earthquake where Q_c is calculated using the following criteria: rectangular area 37.5° < latitude < 40.0° and 19.0° < longitude < 22.0°, time period Δt = [2000, 2003.58] and magnitude $M_{\min} \geq 3.8$. Figure 3c shows the identified critical area using R_n = 90 km. The spatial distribution of $Q_c \leq 0.3$ reveals a reduced area (red-violet color) whose size is comparable to that of the drawn circle surface of radius R = 50 km. Figure 4c shows the estimated occurrence time t_c. The light blue color represents times less than 2003.2 or greater than 2004.3, which correspond to values of Q_c = 1. The green-blue colors represent times close to the origin time and correspond to values of $Q_c \leq 0.25$. For these times, the mean value of the degree of acceleration is m = 0.22, the curvature parameter $c < 0.47$ and the estimated error of occurrence time t_c is less than 1 month if June 2003 is chosen as the last time period in the earthquake catalog.

[31] In order to identify the critical area that participates in the ongoing earthquake process, *Bowman et al.* [1998] proposed an optimal search approach that leads to a usual size of $R_n \gg 100$ km. In this study, however, the radii are constant ($R_n \sim 100$ km, several times a fault length) in order to estimate, for each particular node, the degree to which each area participates in the earthquake preparation phenomenon, and then identify the critical area that can be correlated to the epicentral area of a future event. The result is the identification of a relatively reduced area, comprising at least one part of the epicentral area. In this procedure parameter m was generally restricted to values $0.12 < m < 0.45$. If values outside these limits are permitted, the consequence will be that the size of the revealed area will increase. Additionally, small areas could appear. In Figure 3c, small areas are observed even though $Q_c \ll 1$. These areas became active after the Lefkada event and remain active to this day. This suggests that these areas might be relevant to a future event that may occur in the proximity. This hypothesis is discussed in detail in section 7.2.

5.4. Spatial Discrimination of Seismic Patterns

[32] The spatial characteristics of seismic patterns provide reliable information about stress distribution, identifying earthquake precursors. *Mogi* [1969, 1981] proposed the doughnut pattern before the occurrence of large earthquakes in Japan; the epicentral area was relatively quiet while the periphery exhibited increased seismicity. *Wyss and Habermann* [1988] formulated the precursory seismic quiescence hypothesis, which postulates that the quiet volume overlaps with the main shock source volume. Seismic quiescence before large events has been identified by several authors: the 1992 Landers and Big Bear earthquakes by *Wiemer and Wyss* [1994]; the 1988 Spitak earthquake by *Wyss and Martirosyan* [1998] and by *Zoller et al.* [2002]; the 1995 Kobe earthquake by *Huang et al.* [2001]. *Wiemer and Wyss* [1997] proposed the technique of mapping local recurrence time that can be related to *a*

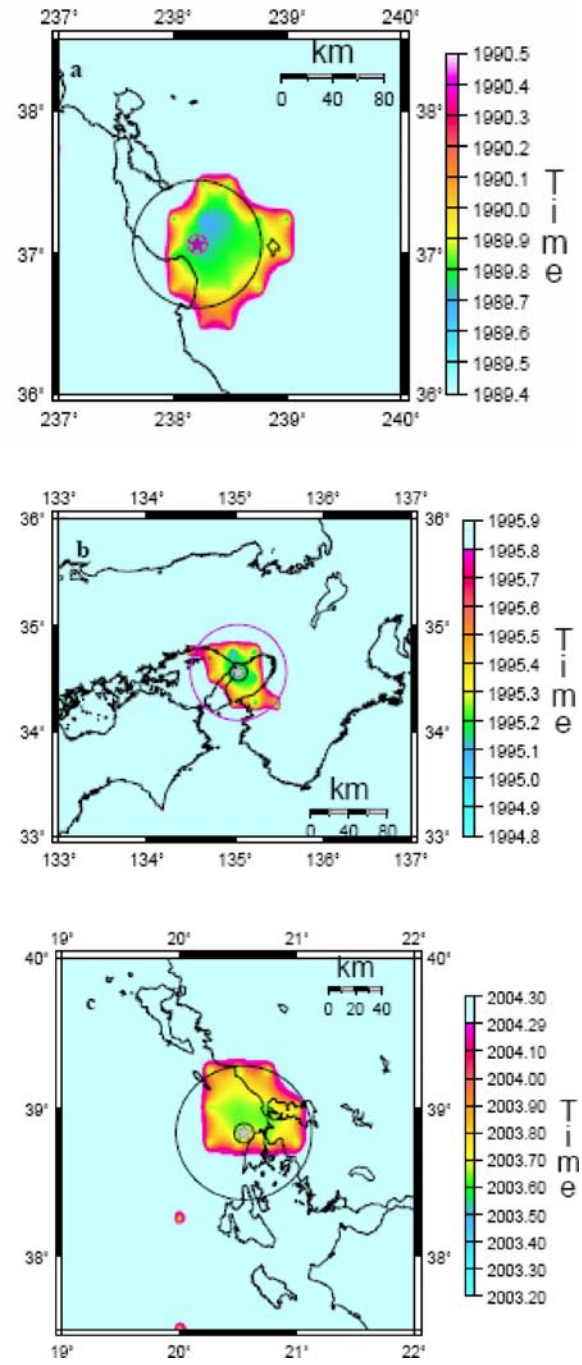

Figure 4. Spatial distribution of the estimated occurrence time (t_c) for the (a) Loma Prieta, (b) Kobe, and (c) Lefkada earthquakes. The star indicates the epicenter of the main event.

and b values. Using this technique, *Oncel and Wyss* [2000] identified major asperities, defined by microseismicity, two decades before the occurrence of the 1999 Izmit earthquake. The method used in this study is similar to the one used by *Oncel and Wyss* [2000]. The difference is that, instead of a and b values, this study uses the energy release by calculating the quality factor Q_s. The area is divided into a grid of about $0.02^\circ \times 0.02^\circ$ spacing, and events that occurred within a time period ΔT are selected. At each node the energy release Q_s is calculated for all events located within a cylindrical volume with radius equal to 10 km.

[33] Because the obtained seismic pattern must be based on real seismicity, the original catalog (without declustering) is used. Such use is not expected to affect significantly the seismic pattern. For the Loma Prieta earthquake, an elliptical area centered at the epicenter, and with radii R_1 = 80 km and R_2 = 120 km, is defined. Events within this elliptical area with magnitude $M_{\min} \geq M_c$ and time period Δt = [1982, 1989.8] are selected, and the quality factor Q_s is calculated at each node. The spatial distribution of the quality factor Q_s is presented in Figure 5a. In Figure 5a, a small circle of radius r_1 = 30 km is also plotted. The seismic pattern shows low values of Q_s represented by blue colors (Q_s is zero for light blue) and high values by orange-red colors. It is evident that the quality factor Q_s within the small circle of radius r_1 (where the main event occurred) has low values indicating low energy release, while at the border areas, higher energy release is observed. These areas are present in the vicinity of the northern and southern edges of the activated fault.

[34] For the Kobe earthquake, a circular area centered at the epicenter with radius R_2 = 150 km, is defined. Events within this area with magnitude $M_{\min} \geq M_c$ and time period Δt = [1984, 1994] are selected and the quality factor Q_s is calculated at each node. The spatial distribution of the quality factor Q_s is presented in Figure 5b. In Figure 5b a small circle of radius r_1 = 50 km is also plotted. The quality factor Q_s within the small circle of radius r_1 indicates low energy release (blue colors), and this is where the main event occurred. A higher level of energy release is observed in the region (orange-red colors) between the small and the large circles, and is mainly concentrated in the vicinity of the edges of the activated fault. For the Lefkada earthquake an elliptical area of radii R_1 = 80 km and R_2 = 100 km, is defined. Events within this elliptical area with magnitude $M_{\min} \geq M_c$ and time period Δt = [1999, 2003.6] are selected, and the quality factor Q_s is calculated at each node. The spatial distribution of the quality factor Q_s is presented in Figure 5c. In Figure 5c a small circle of radius r_1 = 30 is also plotted. The obtained seismic pattern is similar to those of the previous two earthquakes. Within the small circle, where the main event occurred, low energy release is observed (blue colors). A higher energy release is observed in the vicinity of the edges of the activated fault.

[35] The above three applications suggest that a seismic area characterized by low seismic energy release (area defined by the small circle of radius r_1) can be clearly identified around each epicenter. At the same time the surrounding area exhibits a higher level of energy release (area defined between the small and the big circles of radii r_2 and R_2, respectively). Each of these three seismic patterns can be divided into two subareas ("doughnut pattern"), which renders them candidates for the occurrence of a future large earthquake. Moreover, the area of low seismic energy must either be included or coincide with the revealed critical area mentioned previously. Finally, the surrounding area, characterized

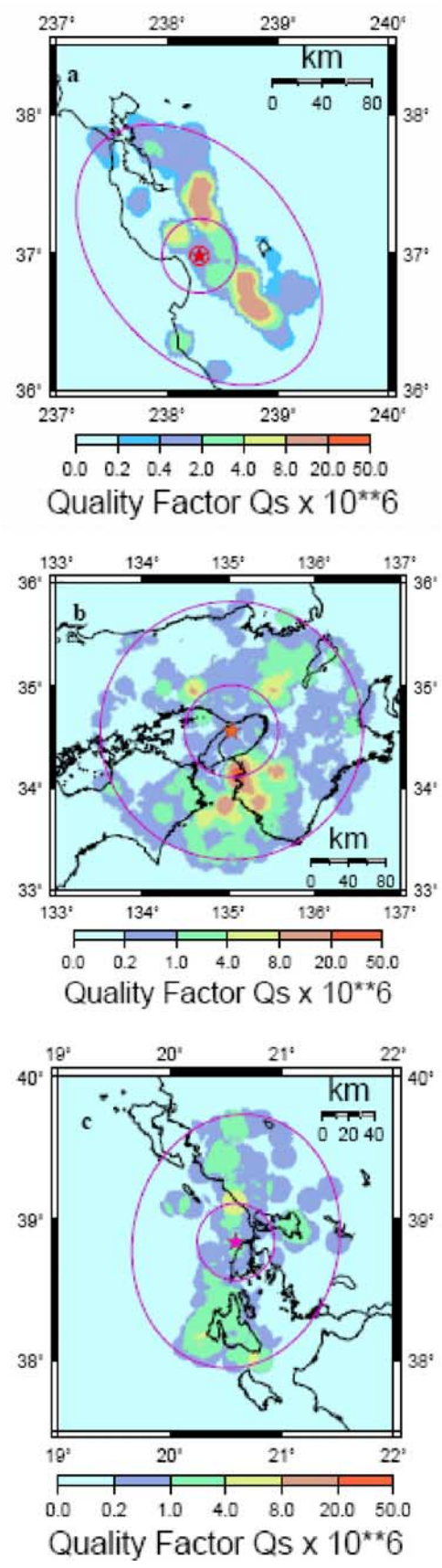

Figure 5. Spatial distribution of the quality factor Q_s for the (a) Loma Prieta, (b) Kobe, and (c) Lefkada earthquakes. The star indicates the epicenter of the main event. For Loma Prieta and Lefkada the azimuths of the ellipses are 140° and 10°, respectively.

by high energy release, shows that most of the energy is concentrated between the two circles (r_2 and R_2), in particular in the vicinity of the edges of the northern and southern ends of the activated fault. Table 1 indicates the source parameters of the analyzed events. The analyses suggest that these seismic patterns might depend on the type of fault.

6. Discussion

[36] For all three earthquakes a clear accelerating seismicity was found with a degree of acceleration $m < 0.30$ and a curvature parameter $c < 0.65$. The estimated time of occurrence t_c was also calculated and tested against the origin time of each event. In order to obtain an error of less than one month, the catalog data must be suspended a few months before the time of the main event. The determination of the time of suspension varies and depends on the seismic pattern. The temporal distribution (Q_t) was analyzed by calculating the variation of energy release in a selected time period. The analysis was based on two observations: the decelerating and the accelerating energy release. These observations are in agreement with each other because each occurs in a different time and space (clearly indicated by the temporal variation of the quality factor Q_t and the spatial distribution of the quality factor Q_s, respectively). As for the acceleration time period, similar observations were found from accelerating seismicity (section 5.1) or temporal analysis (section 5.2). Nevertheless, Q_t could provide more details due to its noncumulative character. In addition, the observed temporal patterns could be modeled using equation (2). For the first period ΔT_d, parameter m must be greater than 1, while for the second Δt_a and third Δt_i parameter m must be less than 1. The decelerating-accelerating sequence (DAMR), which exhibits a certain kind of symmetry, was detected by calculating the quality factor Q_t. This earthquake sequence constitutes a strong double seismic precursor, and for this reason it might be included in an alarm system continuously monitoring the microseismicity of a region.

[37] Concerning the identification of the critical area/time, a grid technique was applied to a selected area around the epicenter in order to identify possible seismic precursors in space/time by calculating the quality factor Q_c. A critical area and time was identified for values $Q_c \ll 1$ for each event. Each critical area includes the epicenter and at least one part of the epicentral area. It is worth noting that the epicenter is not necessarily located at the center of the critical area.

[38] Next, the spatial distribution of energy release was calculated around the revealed critical area. The obtained pattern was divided into two subareas with the central one characterized by low and the surrounding one by higher seismicity. This spatial heterogeneity probably depends on the activation level of the existing fault network in the area, as well as on the type of faulting. Considering a strike-slip

Table 1. Source Parameters for the Loma Prieta, Kobe, and Lefkada Earthquakes[a]

Date	Time, UT	Event	Long (°)	Lat (°)	M	Depth (km)	Strike (°)	Dip (°)	Slip (°)	Ref
18 Oct 1989	0004:15.20	Loma Prieta	121.79W	37.06N	7.1	19	123	71	128	1
16 Jan 1995	2046:51.10	Kobe	135.00E	34.55N	6.9	16	324	70	12	1
14 Aug 2003	0514:00.00	Lefkada	20.56E	38.86N	6.3	9	15	80	170	2

[a]Refs: 1, Harvard; 2, *Papadimitriou et al.* [2006].

mechanism (as in the cases of Kobe and Lefkada), a higher energy release is observed mainly in the vicinity of the edges of the activated faults. This observation could be related to the stress accumulation model (SAM), which can predict the spatial distribution of events before the occurrence of the main shock [*Mignan et al.*, 2006]. Such distributions, occurring in preferential areas, can be considered as foreshock sequences, defining a strong seismic precursor identifier. It should be noted that this kind of observation is detectable but only if the fault network close to the activated fault participates in the ongoing process that produces small and intermediate magnitude events.

[39] The significance of the analysis of spatial distribution of energy release depends on the quality and quantity of the data. The internal area defined by the small circle (epicentral area) could be related to the rupture dimension of the main shock, as in the case of the Kobe earthquake. However, this is not observed for all events. *Savage* [1983] has identified the form of the stress field before an earthquake using a back-slip model. Using the stress accumulation model, *King and Bowman* [2003] calculated the stress distribution through an earthquake cycle close to an activated fault (Coulomb modeling). Stress evolution was calculated for a creeping strike-slip fault, and the observed synthetic seismicity was concentrated mainly in the vicinity of the edges of the fault, while for a reverse type of faulting seismicity was mainly concentrated around the future epicentral area [*Mignan et al.*, 2006]. After the occurrence of the earthquake, the stress pattern switches to the aftershock lobes. The observed stress changes indicate that before the occurrence of the main event the epicentral area remains quiet and stress must be accumulated. In the present study the obtained seismic patterns of the Kobe and Lefkada events (strike-slip type of faulting) are in agreement with these observations. In the Loma Prieta case (oblique thrust type of faulting), high energy release is observed only in the vicinity of the edges of the activated fault instead of the surrounding area. This is probably due to the fact that the rupture exhibits the characteristics of the wider region, which is strike slip. Alternatively, the fault network does not fully participate in the ongoing process.

7. Application in Ionian Sea (Western Greece)

[40] The proposed methodology was applied to the Ionian Sea, which is characterized by intense and complex deformation. The central region is dominated by the Kefallinia-Lefkada dextral transform fault, the southern part by the continental collision between Europe and Africa along the Hellenic arc (subduction zone), and the northern part by the continental collision between the Apulian platform and Europe. The seismic activity for the time period 1960–2006 with magnitude $M \geq 4$ is presented in Figure 6. This region, which is characterized by high seismicity and has suffered in the past by destructive events, is susceptible to a future large earthquake. The most recent large event occurred on 14 August 2003, NW of Lefkada Island. *Papadimitriou et al.* [2006] analyzed this earthquake sequence. Taking into account induced stress transfer, they concluded that the area between Lefkada and Kefallinia could suffer a future main event.

[41] The possibility of the occurrence of an earthquake was examined in the rectangular area 37.5° ≤ latitude ≤ 41.5° and 18° ≤ longitude ≤ 22°. The region was scanned to identify areas in which the quality factor Q_c becomes critical. The analysis presented below identifies two areas in a critical state, the first near the Greek-Albanian border and the second close to Zakynthos Island.

7.1. Greek-Albanian Border Area

[42] The identification of a precursory seismic pattern in space and time was limited to a rectangular area 39.0° <

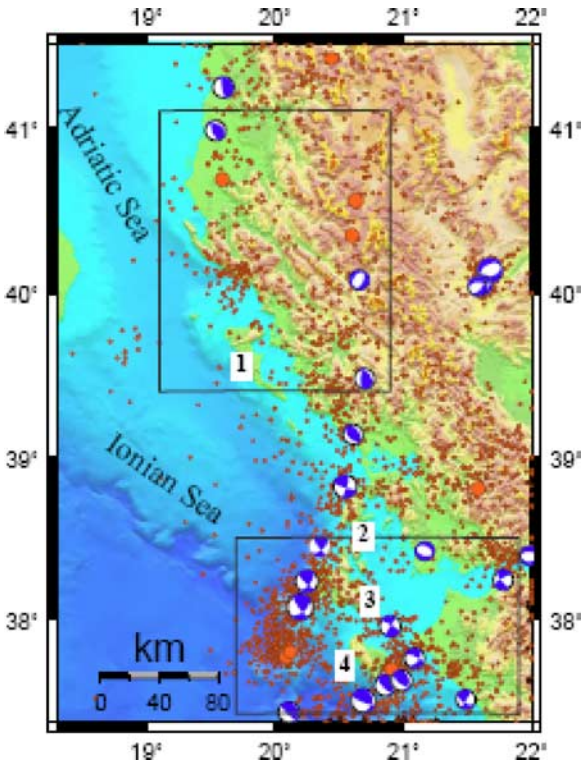

Figure 6. Seismotectonic map of the Ionian Sea and surrounding areas. Large circles indicate earthquakes with $M \geq 5.8$. Fault plane solutions of large earthquakes since 1972: 1, Kerkyra Island; 2, Lefkada Island; 3, Kefallinia Island; and 4, Zakynthos Island. The two rectangles indicate the areas under study.

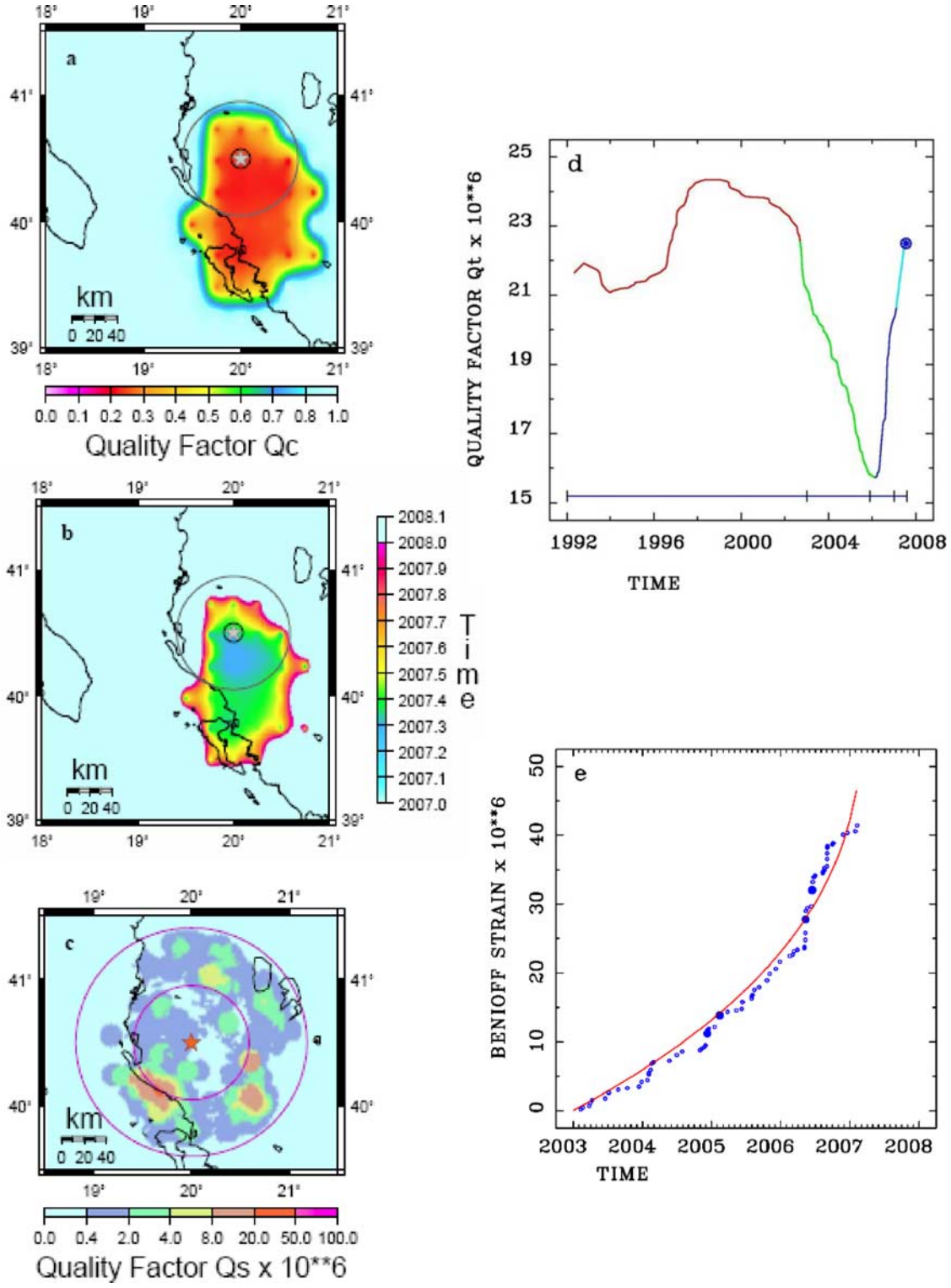

Figure 7. Application to the Greek-Albanian border area: (a) identification of critical area (Q_c); (b) estimated occurrence time (t_c); (c) spatial distribution of energy release (Q_s); (d) temporal variation of energy release (Q_t), the red color indicating the background, the green indicating ΔT_d, the blue indicating Δt_a and the light blue indicating Δt_i time periods, and the star representing the estimated occurrence time of the event; (e) theoretical (curve) and observed (circles) cumulative Benioff strain variation.

latitude < 41.5° and 18.0° < longitude < 21.0°. Events were selected for a time period Δt = [2003, 2007.1] and magnitude $M_{\min} \geq 3.9$. The selected area was divided into a grid of 0.25° × 0.25° spacing. Considering circles whose centers are the nodes, and whose radius is R_n = 90 km, the region was scanned to identify an area in which the quality factor Q_c becomes critical. Figure 7a shows the identified critical area, with values of $Q_c \leq 0.3$ (red-violet colors),

whose size is equivalent to an elliptical area of radii of about $R_1 = 40$ km and $R_2 = 80$ km. Through this procedure the occurrence time t_c was also estimated, and the result is presented in Figure 7b. The light blue color represents times less than 2007.0 or greater than 2008.1, which correspond to values of $Q_c = 1$. The green-blue colors represent times close to $t_c = 2007.3$ and correspond to values of $Q_c \leq 0.25$. For these times, the mean value of the degree of acceleration is $m = 0.39$ and the curvature parameter $c < 0.67$. Next, the area was divided into a grid of $0.02^\circ \times 0.02^\circ$ spacing, and events within a time period ΔT = [1995, 2007.1], focal depth $d_i \leq 80$ km and magnitude $M_{\min} \geq M_c$ were selected. At each node, Q_s was calculated for all events situated within a cylindrical volume with a radius equal to 10 km. The spatial distribution of the energy release is presented in Figure 7c. A circular surface of radius $r_1 = 50$ km centered at [20.0°, 40.5°] is characterized by low (blue colors), while the area between the larger circle of radius $R_1 = 100$ km and the smaller one by high energy release (orange-red colors). The area in which low values of Q_s are observed is included in the revealed critical area. The intense energy release observed north of Kerkyra Island is due to a microseismic sequence that took place in August 2006.

[43] The temporal analysis was conducted using events located within a circle of radius $R_n = 90$ km centered at [20.0°, 40.5°], for a time period Δt = [1980, 2007.1], magnitude $M_{\min} \geq 3.8$, focal depth $d_i < 80$ km and $k = 90$. The quality factor Q_t, for the time period ΔT = [1992, 2003], has a mean value equal to 22.5 $J^{1/2}$ (Figure 7d). It is evident that the energy level has been decreasing continuously since 1999. Considering the value of Q_t in January 2003 as the background level, the energy level reached a minimum level in August 2005, defining the first time period ΔT_d = [2003.0, 2005.9]. After this period, an increase of energy level is observed, defining the second time period Δt_a = [2005.9, 2007.0] followed by an abrupt increase, defining the beginning of the third time period. The end of the identification time is estimated taking into account the value of Q_t, which asymptotically points to the background level (in Figure 7d this point is marked by a star). Thus the estimated identification time period is Δt_i = [2007.0, 2007.6]. The detected seismic precursors have a total duration of $\Delta T \approx 4.6$ years of which $\Delta T_d \approx 2.9$ years are attributed to decelerating, $\Delta t_a \approx 1.1$ years to accelerating seismicity, and $\Delta t_i \approx 0.6$ years to identification time period. If this assumption is correct, then the estimated occurrence time is t_c = 2007.6, with an error of ±0.6 years. The Benioff strain versus time is presented in Figure 7e, assuming a magnitude $M = 6.5$. The strain rate remains approximately constant up to the end of 2006. An abrupt increase is observed in 2006.6, which coincides with the seismic crisis observed north of Kerkyra Island as well as with the increase of energy level Q_t observed during Δt_a. The estimated occurrence time is $t_c = 2007.3$, the mean value of the degree of acceleration $m = 0.35$ and the curvature parameter $c = 0.64$. Similar values obtain when the magnitude is varied ± 0.4. The estimated occurrence time t_c differs from the one calculated by the temporal variation method. This difference can be explained by the widely made observation that an earthquake occurs not at the end of the acceleration period (as in the case of the Lefkada event) but following a relatively short period of decreased seismic activity. In sum, the identified area is in a critical state and a future large earthquake might take place with occurrence time $t_c = 2007.6$ and an error of ± 0.6 year.

7.2. Zakynthos Area

[44] The identification of a precursory seismic pattern in space and time was limited to a rectangular area 37.0° < latitude < 39.5° and 19.0° < longitude < 22.0°. Events were selected for a time period Δt = [2004, 2007.1], focal depth $d_i \leq 80$ km and magnitude $M_{\min} \geq 3.9$. The selected area was divided into a grid of $0.25^\circ \times 0.25^\circ$ spacing. Considering circles whose centers are the nodes, and whose radius is $R_n = 90$ km, the region was scanned to identify an area in which the quality factor Q_c becomes critical. Figure 8a shows the identified critical area, with values of $Q_c \leq 0.3$ (red-violet colors), whose size is equivalent to an elliptical area centered at [20.8°, 38.0°], and radii of about $R_1 = 40$ km and $R_2 = 70$ km. Through this procedure the occurrence time t_c was also estimated, and the result is presented in Figure 8b. The light blue color represents times less than 2007.0 or greater than 2008.1, which correspond to values of $Q_c = 1$. The yellow-green colors represent times close to $t_c = 2007.4$ and correspond to values of $Q_c \leq 0.25$. For these times, the mean value of the degree of acceleration is $m = 0.39$ and the curvature parameter $c < 0.62$.

[45] Then, the area was divided into a grid of $0.02^\circ \times 0.02^\circ$ spacing, and events within a time period ΔT = [1999, 2007.1], focal depth $d_i \leq 80$ km and magnitude $M_{\min} \geq M_c$ were selected. At each node, Q_s was calculated for all events situated within a cylindrical volume with radius equal to10 km. The spatial distribution of the energy release is presented in Figure 8c. The region can be clearly divided into two different subareas that present similar patterns; one west and the other east of Zakynthos Island; the first centered at [20.3, 37.7] and the second at [20.5, 38.1]. Circles of radius $r_1 = 40$ km and centered at each subarea were drawn. The selected subareas exhibit low (blue colors), while the surrounding area exhibits higher levels of energy release. The region presents a complex tectonic setting, mainly dominated by the Hellenic arc (west of Zakynthos) and by the back arc deformation (east of the island). A significant energy release is observed south of Zakynthos Island due to an earthquake sequence during April 2006. Three moderate earthquakes occurred with magnitudes $M = 5.5$, $M = 5.9$, and $M = 5.7$, followed by a significant number of aftershocks.

[46] Regarding the first subarea (west of Zakynthos), the events selected match the following criteria: circle of radius $R_n = 90$ km, time period Δt = [1998, 2007.1], magnitude $M_{\min} \geq 3.7$, focal depth $d_i \leq 80$ km and $k = 120$. The quality factor Q_t, for the time period ΔT = [2000, 2004.5], has a mean value equal to 18.5 $J^{1/2}$ (Figure 8d). It is evident that the energy level has been decreasing continuously since 2004. Considering the value Q_t in March 2004 as the background level, the energy level reaches a minimum in January 2005, defining the first time period ΔT_d = [2004.2, 2005.1]. Following this period an increase of energy level is observed, defining a second time period Δt_a = [2005.1, 2005.6].

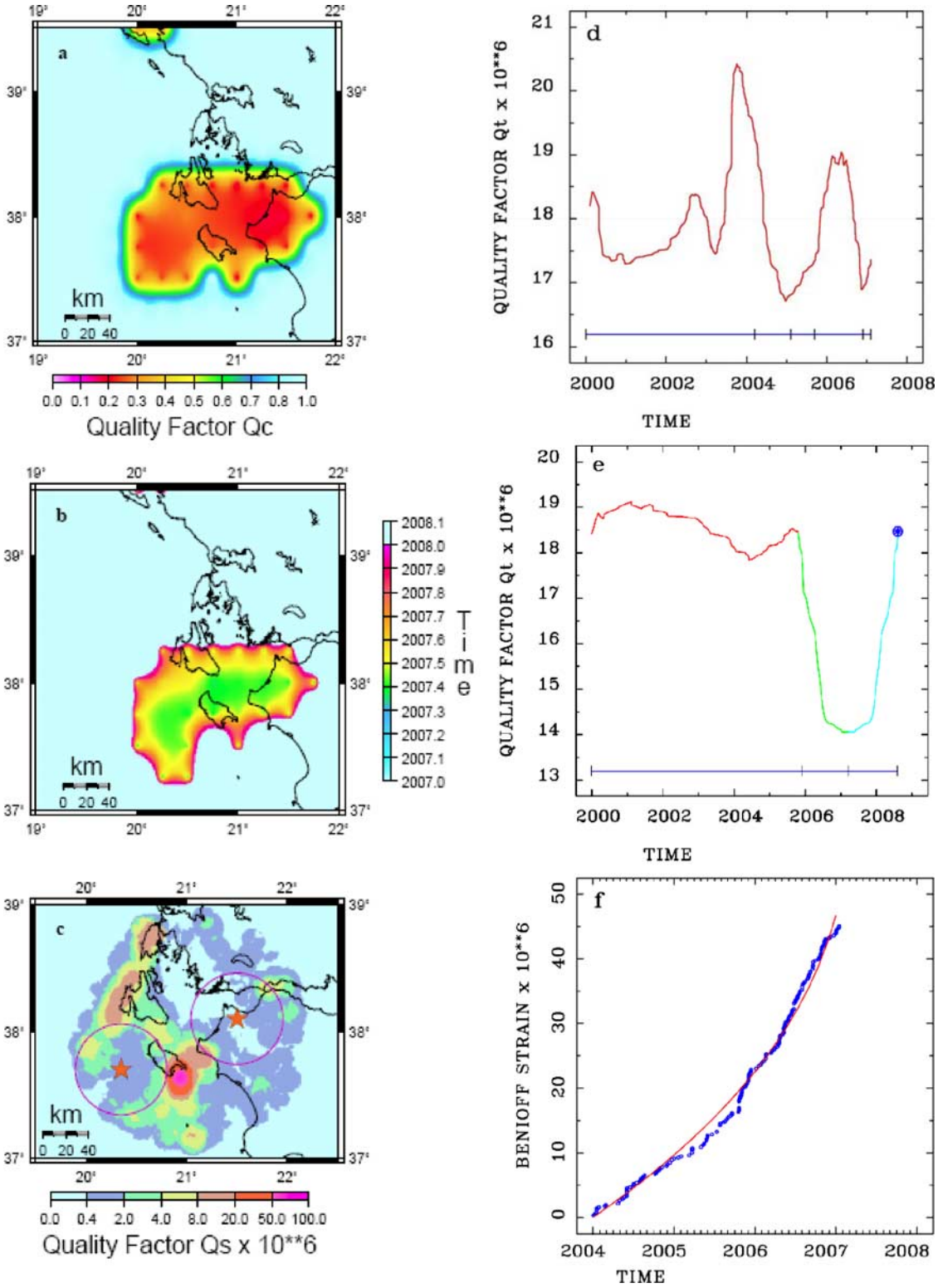

Figure 8. Application to the Zakynthos area: (a) identification of critical area (Q_c); (b) estimated occurrence time (t_c); (c) spatial distribution of energy release (Q_s); (d) temporal variation of energy release west of Zakynthos island (Q_t); (e) temporal variation of energy release east of Zakynthos island (Q_t), the red color indicating the background and the light blue Δt_i time periods, and the star representing the estimated occurrence time of the event; (f) theoretical (curve) and observed (circles) cumulative Benioff strain variation.

At this time an abrupt increase is observed, defining the third time period Δt_i = [2005.6, 2006.0]. The variation of this curve predicted the April 2006 earthquake sequence, mentioned above, associated with occurrence time t_c = 2006.0 estimated with an error of ± 0.4 years. In addition, Q_t reached a new minimum level in December 2006, defining probably the beginning of a new accelerating period.

[47] Concerning the second subarea located east of Zakynthos Island, events were selected using the following criteria: circular area of radius R_n = 90 km, Δt = [1988, 2007.1], magnitude $M_{\min} \geq 3.9$, focal depth $d_i \leq$ 80 km and k = 90. The quality factor Q_t, for the time period ΔT = [2000, 2005.9], has a mean value equal to 18.5 $J^{1/2}$ (Figure 8e). Starting with December 2005 (background level), Q_t continuously decreases until 2007.1, when it reaches probably a minimum level defining the first time period ΔT_d = [2005.9, 2007.1]. As of now, no accelerating time period has been identified (Δt_a = 0). As such the curve variation symmetry is the only factor that can be relied upon. The end of the identification time can be estimated considering the value of Q_t, which asymptotically points to the background level (in Figure 8e this point is marked by a star). Thus the estimated identification time period is Δt_i = [2007.1, 2008.6]. The detected seismic precursors have a total duration of $\Delta T \approx 2.7$ years of which $\Delta T_d \approx 1.2$ years are attributed to decelerating and $\Delta t_i \approx 1.5$ years to identification time period. If this assumption is correct, the estimated occurrence time is t_c = 2008.6 (in Figure 8e this point is represented by a star) with an error of ± 1.5 years.

[48] Finally, the Benioff strain versus time is presented in Figure 8f, assuming a magnitude M = 6.7 (the obtained curve is similar for both subareas). The calculated degree of acceleration is m = 0.38, the curvature parameter c = 0.46 and the estimated occurrence time t_c = 2007.4. In this case the estimated occurrence time t_c differs appreciably from the one calculated by the temporal variation method. The difference is probably due to the fact that the accelerating seismicity exhibits an apparent increase. This shows that the estimated occurrence time calculated by the temporal variation method could be more accurate. In sum, the two subareas exhibit similar characteristics. The identified elliptical area is in a critical state but as of now only the decelerating period has been identified. Taking into account the above results, a large event might take place with occurrence time t_c = 2008.6 with an error of ± 1.5 years.

8. Conclusions

[49] The aim of this study is the identification and quantification of seismic precursors before the occurrence of an earthquake. On the basis of seismic quiescence and accelerating seismicity, both of which are worldwide observations that frequently precede large events, the ''decelerating-accelerating moment release'' (DAMR) earthquake sequence approach is developed. The proposed methodology seeks to discern whether an area can be considered in a critical state and to estimate the magnitude of the event and the critical space and time. The analysis of the data includes four steps: (1) accelerating seismicity, (2) temporal variation of energy release, (3) identification of the critical area/time, and (4) spatial distribution of energy release. The first step models the seismic energy release by fitting the observed seismicity (equation (3)) to the theoretical one (equation (2)). The second step evaluates the temporal energy release by calculating the quality factor Q_t. In the case an earthquake is approaching a double seismic precursor is identified, correlated to the decelerating-accelerating seismicity. The third step identifies the critical area/time associated with an oncoming event by estimating the quality factor Q_c. The fourth step evaluates the spatial distribution of the energy release by calculating the quality factor Q_s. The resulting pattern reveals two areas, one of low and one of high energy release. The area characterized by low seismicity must be correlated to the critical area revealed in the third step. These results can be explained by the stress accumulation model (SAM). The examination of these characteristics of seismic patterns has resulted in the identification of precursors in a space/time window: DAMR, reduced critical area and occurrence time of events. The detection of the double seismic precursor constitutes a strong precursory signal, which can forecast large earthquakes.

[50] According to the analysis of this study, the center of the critical area is the theoretical epicenter of the oncoming event, whose magnitude and occurrence time are estimated in the first step. The theoretical epicenter is defined as a reference geographical point, meaning that the real epicenter is located inside the identified critical area whose size is equivalent to a circular surface of radius $R \sim 50$ km. Thus, the estimated error between the real and the theoretical epicenter is smaller than 100 km, which is generally acceptable. The error between the real and the calculated occurrence time depends on the degree of participation of the fault network in the area. When the critical time Δt_i is identified, the error is smaller than 1 year. The theoretical magnitude of the oncoming event is obtained from the first step (best fit), taking into account the potential of the faults. The estimated magnitude errors are ± 0.4. Even if the obtained errors are acceptable, the proposed methodology needs further refinement.

[51] The methodology was applied to three earthquakes, the 1989 Loma Prieta, the 1995 Kobe, and the 2003 Lefkada, to test its reliability. These events occurred in different seismotectonic regimes and the data was analyzed using three different seismological catalogs. The spatial distribution analysis identified critical areas, covering at least one part of the epicentral area. The temporal analysis revealed a double seismic precursor a few years before the occurrence of the events. This seismic precursor was divided into two time intervals, the decelerating and the accelerating ones. The latter is divided into two subtime periods Δt_a and Δt_i, since from Δt_i it is possible to estimate the error of the occurrence time t_c. Last, the magnitude range $M = M \pm 0.4$ was successfully tested. In effect the errors of the estimated parameters of magnitude, space and origin time are $|M| \leq 0.4$, $|R| \leq 100$ km and $|t_c| \leq 1$ year, respectively. It is noteworthy that the calculated curve, obtained from temporal analysis, is almost symmetrical to the decelerating-accelerating time period. This additional

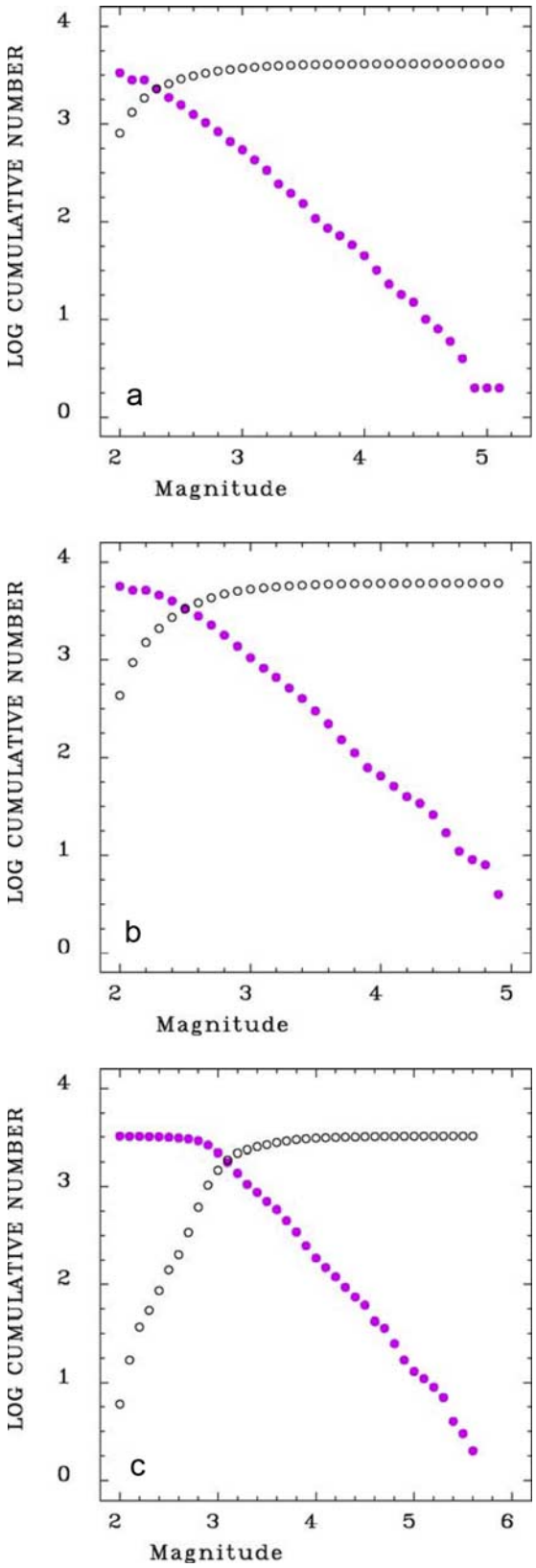

Figure A1. Frequency-magnitude distribution cumulated from above and below for the (a) Loma Prieta, (b) Kobe, and (c) Lefkada earthquakes.

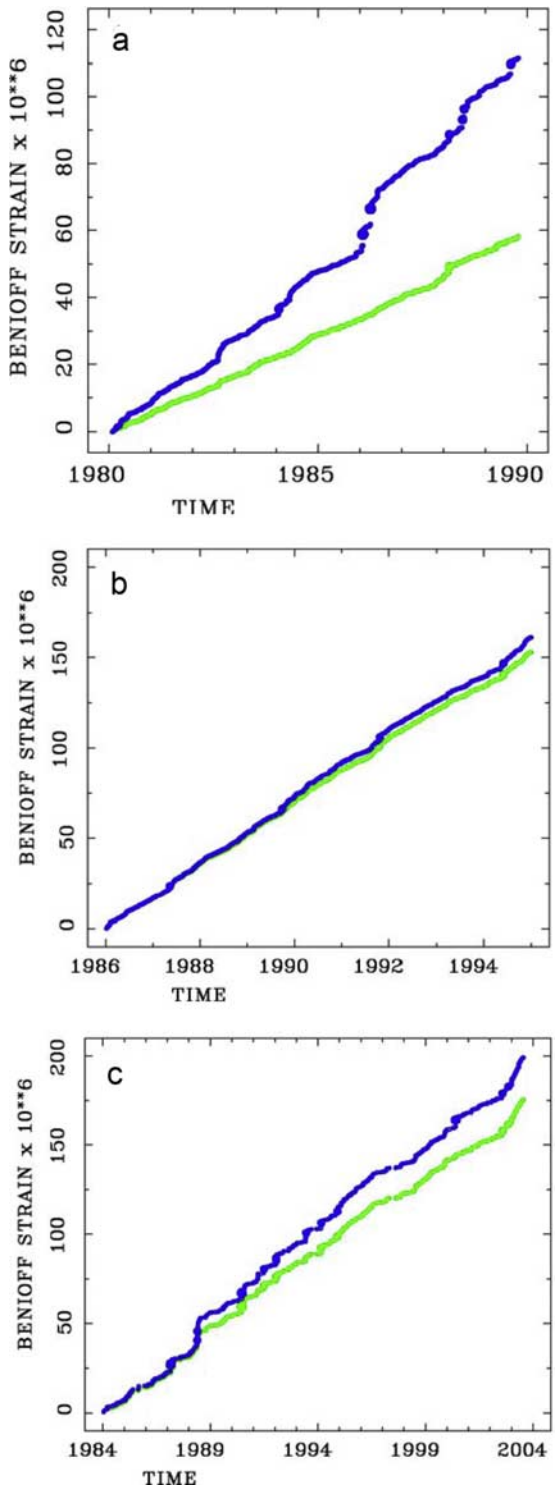

Figure A2. Cumulative Benioff strain variation from original (blue color) and declustered (green color) catalogs for the (a) Loma Prieta, (b) Kobe, and (c) Lefkada earthquakes.

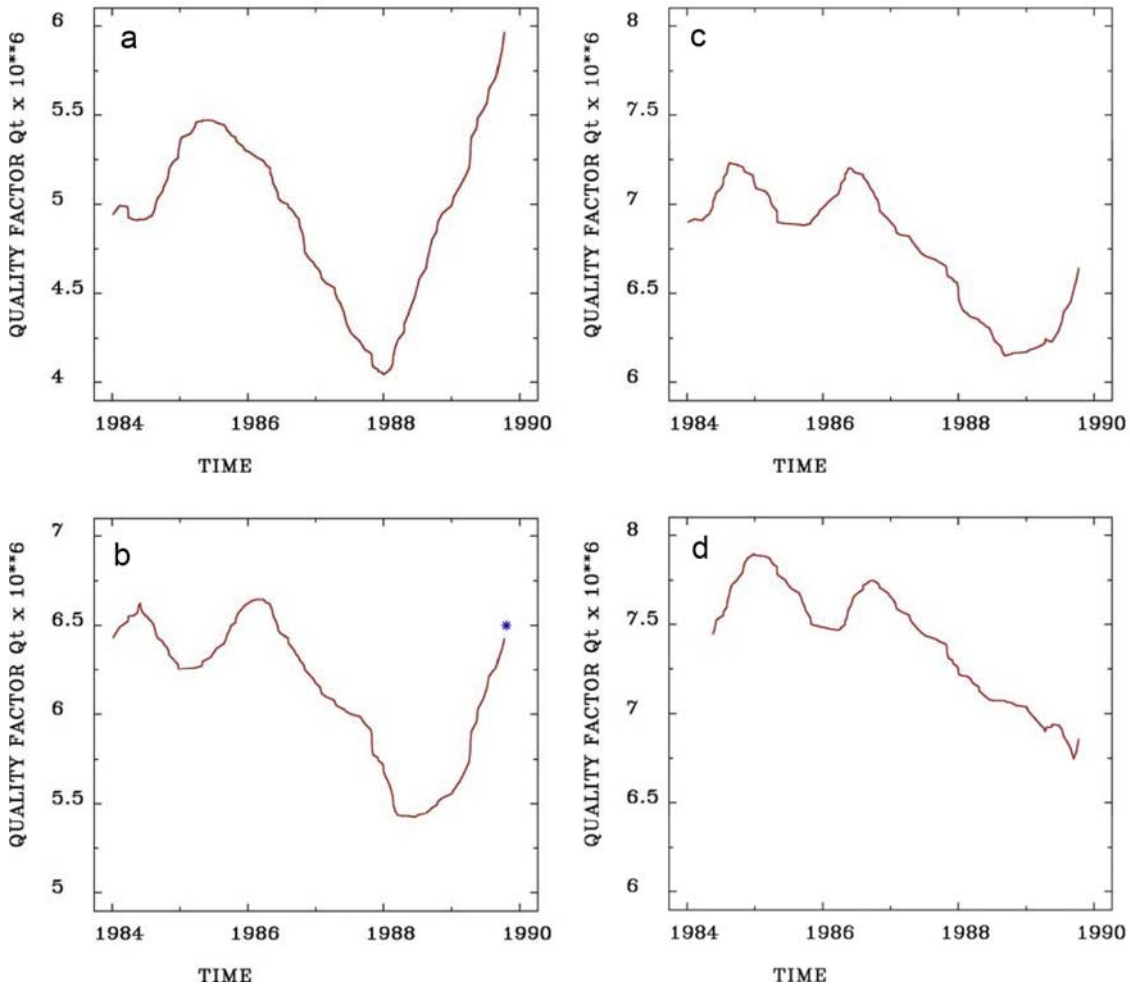

Figure B1. Loma Prieta earthquake. Temporal variation of the quality factor Q_t using (a) $k = 80$, (b) $k = 100$, (c) $k = 110$, and (d) $k = 120$.

datum can be useful for the estimation of the occurrence time.

[52] The last part of the present study concerns the application of the proposed methodology to the Ionian Sea (western Greece). The analysis identified two critical areas, the first located near the Greece-Albania border and the second close to Zakynthos Island. The first one concerns an elliptical area of radii $R_1 = 40$ km and $R_2 = 80$ km centered at [20.0°E, 40.1°N] and the second also an elliptical area of radii $R_1 = 40$ km and $R_2 = 70$ km centered at [20.5°E, 38.0°N]. Within these two areas a future large earthquake could take place.

[53] In summary, the proposed methodology constitutes an initial approach to estimate the earthquake parameters for events that occurred in the past and for events that could happen in the future. In subsequent studies, additional constrains could be incorporated to refine the detection process and increase the reliability of the methodology.

Appendix A: Catalogue Data

[54] In order to detect seismic precursors a seismological catalog must be characterized by independent events due to the tectonic process. Usually, a seismological catalog contains aftershocks and swarms that produce step function changes in the regional seismicity rate. In this study the algorithm of *Reasenberg* [1985] is used to remove these local perturbations. For the Loma Prieta event the rectangular region 36.0° < latitude < 38.5° and 237.0° < longitude < 240.0° and the time period Δt = [1980, 1989.8] are selected. The original catalog comprises 11,081 events with magnitude $M \geq 1.5$. For the Kobe event the rectangular region 33° < latitude < 36° and 133° < longitude < 137° and the time period Δt = [1986, 1994] are selected. The original catalog comprises 6958 events with magnitude $M \geq 1.5$. Finally, for the Lefkada event the rectangular region 37.5° < latitude < 40° and 19° < longitude < 22° and the time period Δt = [1984, 2003.6] are selected. The original catalog comprises 3335 events with magnitude $M \geq 2.5$.

[55] Following, the completeness of the catalogs was evaluated based on the frequency-magnitude distribution cumulated from above and below. For the Loma Prieta the magnitude completeness is $M_c = 2.4$ (Figure A1a), for the Kobe $M_c = 2.6$ (Figure A1b) and for Lefkada $M_c = 3.5$ (Figure A1c). Thus the number of events with $M \geq M_c$ for Loma Prieta, Kobe, and Lefkada are 1999, 2824, and 776, respectively. After declustering, the number of events

becomes 1414, 2774, and 732. The results of the declustering algorithm for the Loma Prieta, Kobe, and Lefkada events are presented in Figures A2a, A2b, and A2c, respectively. In Figures A2a, A2b, and A2c the cumulative Benioff strain variation is presented for the initial catalog and the corresponding declustered one with magnitudes $M \geq M_c$. The difference between the original (blue color) and the declustered (green color) catalogs is that the original presents step function changes while the declustered one exhibits linearity (Figure A2a). In Figures A2b and A2c, there is no significant difference between the original and the declusered catalogs because there are no important step function variations. The result of declustering is a smooth curve for the entire catalog. In all three catalogs, the consequence of declustering is that the cumulative Benioff strain becomes linear (c value is almost 1).

Appendix B: Quality Factor Q_t

[56] The quality factor Q_t is constructed as the sum of $\varepsilon(t)$ of a certain number of k events to quantify the temporal variation of energy release and to detect precursory phenomena. Alternatively it is possible to calculate Q_t by fixing a time period but in this case the result is not as robust. Events within a certain area and time period (about 10 years before the main event) are selected, and Q_t is calculated using the moving window technique. Thus, the quality factor Q_t indicates the degree of variation of the seismic activity and must exhibit similar properties of $s(t)$. For the time period, where the degree of acceleration is $m = 1$, Q_t varies around a mean value (background level). When $m < 1$, Q_t exhibits an increase. The time period between the background seismicity and the acceleration seismicity Q_t shows a deceleration, revealing the seismic quiescence phenomenon. Thus, the temporal variation of the quality factor Q_t, within a properly selected time period, must indicate first a variation around the mean value, and then a deceleration followed by an acceleration time period before the occurrence of the main event. With this in mind, the role of k parameter is to discriminate among the three different time periods. Sometimes the quality factor Q_t exhibits sharp variations, which can be addressed by a smoothing of about 10–20 measurements.

[57] The example of the Loma Prieta earthquake, presented below, shows the difference among four values of k. Figures B1a and B1b show the temporal variation of the quality factor Q_t considering $k = 80$ and $k = 100$, respectively. Figures B1a and B1b show a clear deceleration-acceleration period. As mentioned above, the results from this analysis must be combined with the $s(t)$ variation such that they indicate similar results about (1) acceleration time Δt_a; (2) the identification time Δt_i; and (3) occurrence time t_c. Considering the background level as a reference point, the Q_t variation must asymptotically point to a time whose value is the reference point. This time must be similar to the occurrence time t_c estimated by $s(t)$. Taking these remarks into account, a value of $k = 100$ must be selected. Figures B1c and B1d show the Q_t variation for values $k = 110$ and $k = 120$, respectively. Together, Figures B1c and B1d show that as k increases the accelerating period diminishes to the point where it vanishes.

[58] **Acknowledgments.** The author wishes to acknowledge the contributions of the anonymous reviewers as well as the Associate Editor. Their suggestions and critical comments improved the manuscript substantially.

References

Ben-Zion, Y., and V. Lyakhovsky (2002), Accelerated seismic release and related aspects of seismicity patterns on earthquake faults, *Pure Appl. Geophys.*, *159*, 2385–2412, doi:10.1007/s00024-002-8740-9.

Bowman, D. D., and G. C. P. King (2001), Accelerating seismicity and stress accumulation before large earthquakes, *Geophys. Res. Lett.*, *28*, 4039–4042, doi:10.1029/2001GL013022.

Bowman, D. D., G. Ouillon, C. G. Sammis, A. Sornette, and D. Sornette (1998), An observational test of the critical earthquake concept, *J. Geophys. Res.*, *103*, 24,359–24,372, doi:10.1029/98JB00792.

Bufe, C. G., and D. J. Varnes (1993), Predictive modeling of the seismic cycle of the Great San Francisco Bay region, *J. Geophys. Res.*, *98*, 9871–9883, doi:10.1029/93JB00357.

Huang, J., and D. L. Turcotte (1988), Fractal distributions of stress and strength and variations of b-value, *Earth Planet. Sci. Lett.*, *91*, 223–230, doi:10.1016/0012-821X(88)90164-1.

Huang, Q., G. A. Sobolev, and T. Nagao (2001), Characteristics of the seismic quiescence and activation patterns before the $M = 7.2$ Kobe earthquake, January 17, 1995, *Tectonophysics*, *337*, 99–116, doi:10.1016/S0040-1951(01)00073-7.

Jaume, S. C., and L. R. Sykes (1999), Evolving towards a critical point: a review of accelerating seismic moment/energy release rate prior to large and great earthquakes, *Pure Appl. Geophys.*, *155*, 279–306, doi:10.1007/s000266.

Kagan, Y. Y., and D. D. Jackson (1991), Long-term earthquake clustering, *Geophys. J. Int.*, *104*, 117–133, doi:10.1111/j.1365-246X.1991.tb02498.x.

Kagan, Y. Y., and L. Knopoff (1980), Spatial distribution of earthquakes: The two-point correlation function, *Geophys. J. R. Astron. Soc.*, *62*, 303–320.

Kanamori, H., and D. L. Anderson (1975), Theoretical basis of some empirical relations in seismology, *Bull. Seismol. Soc. Am.*, *65*, 1073–1095.

Keilis-Borok, V. I., and V. G. Kossobokov (1990), Premonitory activation of earthquake flow algorithm M8, *Phys Earth Planet Inter*, *61*, 73–83, doi:10.1016/0031-9201(90)90096-G.

King, G. C. P., and D. D. Bowman (2003), The evolution of regional seismicity between large earthquakes, *J. Geophys. Res.*, *108*(B2), 2096, doi:10.1029/2001JB000783.

King, G. C. P., R. S. Stein, and J. Lin (1994), Static stress changes and the triggering of earthquakes, *Bull. Seismol. Soc. Am.*, *84*, 935–953.

Main, I. G. (1999), Applicability of time-to-failure analysis to accelerated strain before earthquakes and volcanic eruptions, *Geophys. J. Int.*, *139*, F1–F6, doi:10.1046/j.1365-246x.1999.00004.x.

Mignan, A., D. D. Bowman, and G. C. P. King (2006), An observational test of the origin of accelerating moment release before large earthquakes, *J. Geophys. Res.*, *111*, B11304, doi:10.1029/2006JB004374.

Mogi, K. (1969), Some features of the recent seismic activity in and near Japan: 2. Activity before and after great earthquakes, *Bull. Earthquake Res. Inst. Univ. Tokyo*, *47*, 395–417.

Mogi, K. (1981), Seismicity in western Japan and long term earthquake forecasting, in *Earthquake Prediction: An International Review*, *Maurice Ewing Ser.*, vol. 4, edited by D. W. Simpson, and P. G. Richards, pp. 43–51, AGU, Washington, D. C.

Oncel, A. O., and M. Wyss (2000), The major asperities of the 1999 Mw = 7.4 Izmit earthquake defined by the microseismicity of the two decades before it, *Geophys. J. Int.*, *143*, 501–506, doi:10.1046/j.1365-246X.2000.00211.x.

Papadimitriou, P. (2002), Seismicity and earthquake prediction in the Aegean: Some encouraging results, paper presented at 2nd Symposium in Geophysics and Seismology, Univ. of Athens, Athens, Greece.

Papadimitriou, P. (2004), Accelerating strain rate prior to large earthquakes, paper presented at XXIX General Assembly of ESC, Eur. Seismol. Comm., Potsdam, Germany.

Papadimitriou, P., G. Kaviris, and K. Makropoulos (2006), The $M_w = 6.3$ 2003 Lefkada earthquake (Greece) and induced stress transfer changes, *Tectonophysics*, *423*, 73–82, doi:10.1016/j.tecto.2006.03.003.

Papazachos, B., and C. Papazachos (2000), Accelerated preshock deformation of broad regions in the Aegean area, *Pure Appl. Geophys.*, *157*, 1663–1681, doi:10.1007/PL00001055.

Papazachos, B. C., A. S. Savvaidis, C. B. Papazachos, and G. F. Karakaisis (2002), Precursory seismic crustal deformation in the area of southern Albanides, *J. Seismol.*, *6*, 237–245, doi:10.1023/A:1015663224435.

Papazachos, C. B., G. F. Karakaisis, E. M. Scordilis, and B. C. Papazachos (2004), Probabilities of activation of seismic faults in critical regions of the Aegean area, *Geophys. J. Int.*, *159*, 679–687, doi:10.1111/j.1365-246X.2004.02407.x.

Papazachos, C. B., G. F. Karakaisis, E. M. Scordilis, and B. C. Papazachos (2005), Global observational properties of the critical earthquake model, *Bull. Seismol. Soc. Am.*, *95*, 1841–1855, doi:10.1785/0120040181.

Papazachos, C. B., G. F. Karakaisis, E. M. Scordilis, and B. C. Papazachos (2006), New observational information on the precursory accelerating and decelerating strain energy release, *Tectonophysics*, *423*, 83–96, doi:10.1016/j.tecto.2006.03.004.

Reasenberg, P. A. (1985), Second-order moment of central California seismicity, 1969–1982, *J. Geophys. Res.*, *90*, 5479–5495, doi:10.1029/JB090iB07p05479.

Reasenberg, P. A., and R. W. Simpson (1992), Response of regional seismicity to the static stress change produced by the Loma Prieta earthquake, *Science*, *255*, 1687–1690, doi:10.1126/science.255.5052.1687.

Rundle, J. B., W. Klein, D. L. Turcotte, and B. D. Malamud (2000), Precursory seismic activation and critical-point phenomena, *Pure Appl. Geophys.*, *157*, 2165–2182, doi:10.1007/PL00001079.

Saleur, H., C. G. Sammis, and D. Sornette (1996), Discrete scale invariance, complex fractal dimensions, and log-periodic fluctuations in seismicity, *J. Geophys. Res.*, *101*, 17,661–17,677, doi:10.1029/96JB00876.

Sammis, C. G., D. D. Bowman, and G. C. P. King (2004), Anomalous seismicity and accelerating moment release preceding the 2001 and 2002 earthquakes in northern Baja California, Mexico, *Pure Appl. Geophys.*, *161*, 2369–2378, doi:10.1007/s00024-004-2569-3.

Savage, J. C. (1983), A dislocation model of strain accumulation and release at a subduction zone, *J. Geophys. Res.*, *88*, 4948–4996, doi:10.1029/JB088iB06p04984.

Smirnov, V. B. (1998), Earthquake catalogs: Evaluation of data completeness, *J. Volcanol. Seismol.*, *19*, 433–446.

Sobolev, G. A., and Y. S. Tyupkin (1999), Precursory phases, seismicity precursors, and earthquake prediction in Kamchatka, *J, Volcanol. Seismol.*, *20*, 615–627.

Sornette, A., and D. Sornette (1990), Earthquake rupture as a critical point: Consequences for telluric precursors, *Tectonophysics*, *179*, 327–334, doi:10.1016/0040-1951(90)90298-M.

Sornette, D., and C. G. Sammis (1995), Complex critical exponents from renormalization group theory of earthquakes: Implications for earthquake predictions, *J. Phys. I*, *5*, 607–619, doi:10.1051/jp1:1995154.

Stein, R. S. (1999), The role of stress transfer in earthquake occurrence, *Nature*, *402*, 605–609, doi:10.1038/45144.

Sykes, L. R., and S. Jaume (1990), Seismic activity on neighboring faults as a long term precursor to large earthquakes in the San Francisco Bay area, *Nature*, *348*, 595–599, doi:10.1038/348595a0.

Tiampo, K. F., J. B. Rundle, and W. Klein (2006), Premonitory seismicity changes prior to the Parkfield and Coalinga earthquakes in southern California, *Tectonophysics*, *413*, 77–86, doi:10.1016/j.tecto.2005.10.011.

Toda, S., and R. Stein (2003), Toggling of seismicity by the 1997 Kagoshima earthquake couplet: A demonstration of time-dependent stress transfer, *J. Geophys. Res.*, *108*(B12), 2567, doi:10.1029/2003JB002527.

Wiemer, S., and M. Wyss (1994), Seismic quiescence before the Landers (M = 7.5) and Big Bear (M = 6.5) 1992 earthquakes, *Bull. Seismol. Soc. Am.*, *84*, 900–916.

Wiemer, S., and M. Wyss (1997), Mapping the frequency magnitude distribution in asperities: An improved technique to calculate recurrence times?, *J. Geophys. Res.*, *102*, 15,115–15,128, doi:10.1029/97JB00726.

Wyss, M., and R. E. Habermann (1988), Precursory seismic quiescence, *Pure Appl. Geophys.*, *126*, 319–332, doi:10.1007/BF00879001.

Wyss, M., and A. H. Martirosyan (1998), Seismic quiescence before the M7, 1988, Spitak earthquake, Armenia, *Geophys. J. Int.*, *134*, 329–340, doi:10.1046/j.1365-246x.1998.00543.x.

Zoller, G., S. Hainzl, and J. Kurths (2001), Observation of growing correlation length as an indicator for critical point behavior prior to large earthquakes, *J. Geophys. Res.*, *106*, 2167–2175, doi:10.1029/2000JB900379.

Zoller, G., S. Hainzl, J. Kurths, and J. Zschau (2002), A systematic test on precursory seismic quiescence in Armenia, *Nat. Hazards*, *26*, 245–263, doi:10.1023/A:1015685006180.

P. Papadimitriou, Department of Geophysics, University of Athens, Panepistimiopolis, Zografou, 15784, Greece. (ppapadim@geol.uoa.gr)